Chemical forms of calcium in Ca,Zn- and Ca,Cd-containing grains excreted by tobacco trichomes

Géraldine Sarret[1], Marie-Pierre Isaure, Matthew A. Marcus, Emiko Harada, Yong-Eui Choi, Sébastien Pairis, Sirine Fakra and Alain Manceau

Géraldine Sarret, Marie-Pierre Isaure, Emiko Harada and Alain Manceau. Environmental Geochemistry Group, LGIT, University of Grenoble and CNRS, BP 53, 38041 Grenoble cedex 9, France

Matthew A. Marcus and Sirine Fakra. Advanced Light Source (ALS), Lawrence Berkeley National Lab, MS 6-100, Berkeley, CA 94720, USA

Emiko Harada and Yong-Eu Choi. Division of Forest Resources, College of Forest Sciences, Kangwon National University, Chunchon 200-701, Kangwon-do, Korea

Sébastien Pairis. Institut Néel CNRS-UJF, Dept. Matière Condensée, Matériaux et Fonctions, Pôle Instrumentation (Microscopie Electronique), 25 av. des Martyrs, BP 166, 38042 Grenoble cedex 9, France

[1] Corresponding author. Email: geraldine.sarret@ujf-grenoble.fr

Tel: (33) 4 76 82 80 21, Fax: (33) 4 76 82 81 01

Abstract

Tobacco (*Nicotiana tabacum* L. cv. Xanthi) plants exposed to toxic levels of zinc and cadmium excrete metals through their leaf trichomes (epidermal hairs) as Zn,Ca- and Cd,Ca-containing grains. Little is known about the nature and formation mechanism of these precipitates. The chemical, crystalline, and non-crystalline compositions of individual grains produced by tobacco were studied by scanning electron microscopy coupled with energy dispersive X-ray analysis (SEM-EDX), micro-X-ray diffraction (μXRD) and calcium K-edge micro X-ray absorption near edge structure (μXANES) spectroscopy. Zinc is predominantly incorporated in calcite, and cadmium in calcite and vaterite. Aragonite, which occurs occasionally, does not seem to contain trace metals. In addition to being precipitated in its three possible polymorphic forms, calcite, aragonite and vaterite, calcium also is speciated as amorphous $CaCO_3$ and possibly organic Ca in some grains. Most often, a particular grain consists of two or more crystalline and non-crystalline phases. The observed variability of intra- and inter-grain elemental and phase composition suggests that this biomineralization process is not constrained by biological factors, but instead results from thermodynamically and kinetically controlled reactions. This study illustrates the potential of laterally resolved X-ray synchrotron radiation techniques (μXRD and μXANES) to study biomineralization and metal immobilization processes in plants.

Introduction

Recently, a novel original mechanism of Zn and Cd detoxification was described in tobacco (*Nicotiana tabacum* L. cv. Xanthi). Tobacco exposed to Cd excreted Cd,Ca-containing grains through leaf trichomes (1, 2), and a similar excretion of Zn,Ca-containing grains was observed under Zn exposure (3). Trichomes are specialized epidermal structures. In tobacco, they are glandular and excrete various organic substances including nicotine and resins. Such detoxification process may have implication in human health since smoking is one of the principal routes of exposure to heavy metals, and also in phytoremediation as tobacco is a candidate species for phytoextraction.

The morphology, elemental composition, mineralogy as well as Zn and Cd speciation in the grains were investigated by scanning electron microscopy coupled with energy dispersive X-ray analysis (SEM-EDX), micro-X-ray fluorescence (µXRF), micro-X-ray diffraction (µXRD), Zn K-edge micro extended X-ray absorption fine structure (µEXAFS) (3) and Cd L_{III} edge micro X-ray absorption near edge structure (µXANES) spectroscopy (Isaure et al., in prep.). Calcium was always the major component. µXRD analyses revealed the presence of calcite, and less frequently vaterite and aragonite, two other $CaCO_3$ polymorphs. Calcium oxalate mono and dihydrate were found occasionally. Calcite and vaterite were substituted by cations, probably Zn, Cd and possibly Mn and Mg. Zn µEXAFS confirmed the occurrence of Zn-substituted calcite, and evidenced Zn associations with other phases including organic compounds, silica and phosphate (3). Cd µXANES showed that cadmium was a Ca substituent in calcite and vaterite and/or sorbed on the surface of these minerals (Isaure et al., in prep.).

The mechanism of formation of these grains remains unclear. Biogenic minerals may result from a controlled biomineralization process leading to well defined minerals and shapes. They may also be “biologically induced”, which means that an organism promotes the precipitation, but

43 does not control the crystallization process (4). In the present case, grains could result from the
44 exudation of a liquid containing the various metals and substances, and precipitation of the
45 various solid phases due to water evaporation. Alternatively, they might be formed intracellularly
46 and excreted thereafter as suggested by Choi et al. (5). The purpose of this study is to better
47 characterize the structure and composition of the grains. Grains excreted by tobacco under
48 various Zn, Cd and Ca exposure conditions were investigated by SEM-EDX, µXRD and Ca K-
49 edge µXANES spectroscopy. Results of these complementary approaches are compared, and a
50 hypothesis for the formation of the grains is proposed in light of these data.
51

52 **Experimental**

53 *Materials*

54 Plant culture and grain collection procedure have been described previously (3). Briefly, tobacco
55 plants were grown in hydroponic conditions and exposed for 5 weeks to Zn or Cd, with or
56 without a supplement of Ca (Table 1). A control condition with Ca only was also tested. Then,
57 grains were collected by washing the leaves in ultrapure water and centrifugating the suspension.
58 Several Ca-containing reference compounds were used for the Ca XANES data analysis.
59 Calcite, vaterite and Cd-containing vaterite were synthesized at room temperature according to a
60 modified protocol of Paquette and Reeder (6, 7). Briefly, an aqueous solution (500 mL)
61 containing 10 mM $CaCl_2$ and 1.8 M NH_4Cl was placed in a glass reactor, an EPPENDORF tube
62 containing solid ammonium carbonate was allowed to float at the surface of the solution, and the
63 reactor was closed and kept unstirred. NH_4Cl was used as a background electrolyte to provide a
64 high ionic strength. Initial pH was 4.9. The decomposition of ammonium carbonate produces
65 NH_3(g) and CO_2(g), which dissolve into the solution, simultaneously increasing pH and
66 alkalinity. The supersaturation of the solution induces the formation and growth of $CaCO_3$

67 crystals. Continuous sublimation of NH_3(g) buffers the solution around pH = 7.9. After 13 days,
68 the reactor contained rhombohedral crystals and spherical particles attached on the surface of the
69 glass. The two types of particles were separated and characterized by XRD. Rhombohedral
70 crystals corresponded to calcite, and spherical particles to vaterite. For the synthesis of Cd-
71 containing vaterite, the same procedure was used except that after 13 days, when crystal size
72 amounted to 150-200 μm in diameter, the $CaCl_2$-NH_4Cl solution was progressively doped with
73 0.1 M $CdCl_2$ to a total concentration of 100 μM Cd in order to incorporate Cd as a Ca substituent
74 in vaterite (6, 7). The progressive addition of $CdCl_2$ kept the solution undersaturated with respect
75 to otavite ($CdCO_3$). After 7 days, the particles were collected and separated. Spherical particles
76 were identified as Cd-containing vaterite by XRD and μXRF. The Cd content was a few tens
77 ppm based on μXRF analysis.
78 Aragonite was a natural specimen. The XANES spectrum for synthetic amorphous $CaCO_3$ was
79 provided by Y. Politi (8). Ca oxalate monohydrate (whewellite) was purchased from Aldrich. A
80 solution containing 0.5 M $Ca(NO_3)_2$ at pH 2.6 was used as a reference for aqueous Ca^{2+}. The
81 phase purity of all crystalline samples was checked by XRD prior to XANES analysis.
82
83 *Electron microscopy*
84 The morphology and the chemical composition of the grains were studied by SEM-EDX using a
85 Jeol-JSM 840A equipped with a Kevex Si(Li) detector. The chamber pressure was 10^{-6}-10^{-5} Torr,
86 and the accelerating voltage 20 kV. Grains were mounted on kapton tape or on carbon tape, then
87 fixed on carbon stubs and coated with carbon. Images were taken at a magnification of 500 to
88 10000. EDX spectra were recorded on prominent spots of the grains to optimize the detection.
89
90 *Micro-XRF, μXRD and μXANES*

The μXRF, μXRD and Ca K-edge μXANES measurements were performed on beamline 10.3.2 of the Advanced Light Source (ALS, Berkeley, CA) (9). The grains were spread on kapton tape and analyzed at room temperature and pressure. First, each grain was mapped by μXRF. Then, μXANES and μXRD and data were recorded on the Zn-richest region for the Zn and Zn + Ca treatments, on the Cd-richest region for the Cd and Cd + Ca treatment, and on the Ca-richest region for the Ca treatment. μXRF data were collected at 10 keV with a beam size of 5 × 5 μm. The same X-ray spot size was used for Ca μXANES. Fluorescence X-ray yield was measured with a 7-element Ge solid-state detector. The spectra were recorded between 3900 to 4400 eV. μXRD patterns were recorded at an incident energy of 17 keV with a beam size of 16 × 7 μm. More experimental details are given in (3). Ca XANES reference spectra were recorded at room temperature on beamline ID21 at the European Synchrotron Radiation Facility (ESRF, Grenoble, France). Each spectrum is the average of two to three spectra, each about 15 minutes long.

XRD and XANES data treatment

The XRD data treatment was performed as described previously (3). Briefly, after calibration with alumina, two dimensional XRD patterns were integrated to one-dimensional patterns for peak assignment. For substituted calcite crystals, the unit cell parameters *a* and *c* were refined, and the stoichiometry of the substituent was estimated from these two parameters using the Vegard law (10) with calcite, smithsonite ($ZnCO_3$) and otavite ($CdCO_3$) as end-members for the Ca-Zn and Ca-Cd solid solutions. This approach cannot be used for substituted vaterite because of the absence of a $CdCO_3$ structural analogue of vaterite.

XANES spectra were processed using WinXAS (11). All spectra were energy calibrated

with respect to calcite (inflection point for this reference set to 4042.6 eV). The collected scans were averaged; background subtracted and normalized using linear (pre-edge) or cubic (post-edge) polynomials. XANES spectra were then fitted by linear combinations using calcite, aragonite, vaterite, Cd-containing vaterite, amorphous $CaCO_3$, aqueous Ca^{2+} and Ca oxalate monohydrate reference spectra. The quality of the fits was quantified by the normalized sum-squares residuals $NSS = \Sigma(\mu_{experimental} - \mu_{fit})^2 / \Sigma(\mu_{experimental})^2 \times 100$, in the 4000-4150 eV range, where μ is the normalized absorbance. An energy shift of ± 0.5 eV maximum and a correction of slope were allowed to account for the energy resolution of the monochromator and for possible inconsistencies in data processing. For some spectra, linear combination (LC) fitting did not provide satisfactory results, and over-absorption effects were suspected based on the comparison of these spectra with the standards. Therefore, each spectrum was fitted with and without a correction of over-absorption using a simple model (12). This model assumes that the smooth part of the resonant absorption is a constant fraction of the non-resonant background (which is a reasonable assumption in the XANES region) and that the sample is infinitely thick, *i.e.*, totally absorbs the incident beam (which is probably true considering the energy range and the size and global composition of the grains). The equation used is:

$$y_{experimental} = (1 + a) / (1 + a \cdot y_{corrected}) \qquad (1)$$

where y is the normalized resonant absorbance, which equals 0 below the edge and oscillates around 1 above the edge, and $a = \mu_{resonant} / (\mu_{non\ resonant} + \mu_{fluorescence})$ where $\mu_{resonant}$, $\mu_{non\ resonant}$ and $\mu_{fluorescence}$ are the three components of the absorbance μ. Equation (1) can be solved as:

$$y_{corrected} = y_{experimental} / (1 + a\,(1 - y_{experimental})) \qquad (2)$$

135 The over-absorption parameter *a* equals 0 in the absence of over-absorption effect, and
136 increases with this effect. Because of the sample heterogeneity, the precise composition of the
137 sample is not known, so *a* is an adjusted parameter.
138
139 **Results**
140 The morphology of the grains as observed by SEM varied considerably. The grains varied from
141 10 µm to 150 µm in diameter. Each grain is an aggregate of different types of particles. The first
142 type is micro faceted crystallites (Insets in Fig. 1a and 1b) and the second type is globular
143 structures of various sizes (from 2 to 50 µm, Fig. 1c, 1d and 1e). Some grains such as Zn2 (Fig.
144 1c) seem visually less crystalline. The elemental composition of the grains varies from one grain
145 to another, and within the same grain. Ca was always the major component regardless of the plant
146 metal treatment conditions. Minor elements include Mg, Si, P, Cl, K, and Zn or Cd depending on
147 the plant treatment (Fig. 1). The high Si peaks observed in Fig. 1a to 1d are attributed to kapton
148 tape on which the grains were mounted. Silicon is not detected in the grain presented in Fig. 1e
149 (mounted on carbon tape). However, Si was found in small amount in some grains (not presented
150 in this study), as well as Mn.
151 Our previous study using µXRD (3) showed that grain ZnCa3 contained substituted calcite and
152 aragonite, that grain ZnCa4 contained substituted calcite, and that grain Zn2 did not contain
153 crystalline phases. The two-dimensional µXRD patterns for grains ZnCa5 and Zn3 show that the
154 Bragg reflections for these two grains consist of small arcs of Debye-Scherrer rings, indicating
155 that the grains are composed of micrometer-size mosaic crystals (Fig. 2b). All reflections
156 correspond to substituted calcite, and the major Ca substituent is Zn based on µXRF (Fig. 2a).
157 Note that although Ca is the major element, the Ca Kα peak has a low intensity relative to the Zn
158 Kα peak due to air absorption and the lower fluorescence yield of Ca *vs*. Zn. The refined unit cell

159 parameters *a* and *c* for grain ZnCa5 and Zn3 were 4.97 and 16.97 Å, and 4.95 and 16.83 Å,
160 respectively, compared to 4.9896 and 17.0610 Å for pure calcite. The calculated formulae using
161 the Vegard law were $Ca_{0.95}Zn_{0.05}CO_3$ and $Ca_{0.89}Zn_{0.11}CO_3$, respectively. The difference in the Zn
162 stoichiometry coefficient obtained using parameters *a* and *c* was ± 0.01. The µXRD results for
163 the Cd-containing grains will be presented separately together with Cd L_{III}-XANES data (Isaure
164 et al., in preparation). Briefly, the grains CdCa2 and Cd10 contain micrometer crystals of
165 substituted calcite and finer (nanometer sized) crystals of substituted vaterite. Grain CdCa3
166 contains nano-crystals of substituted vaterite only. Finally, no crystalline phases were detected in
167 grain CdCa6. For Cd- substituted calcite, the Vegard law provides an imprecise estimation of Cd
168 stoichiometry because the contrast in ionic radius between Cd and Ca is small (0.95 Å for Cd^{2+}
169 and 1.00 Å for Ca^{2+} compared to 0.74 Å for Zn^{2+}) (13). For instance, the substitution rate for
170 grain CdCa2 could be anywhere between 30 and 80%. It was not possible to calculate the
171 stoichiometry of Cd in vaterite because of the absence of a Cd end member (see the Experimental
172 section).
173 Calcium being the major element in the grains, Ca K-edge µXANES spectroscopy was then
174 performed to get some insights on the composition of the grains, and test for the presence of
175 amorphous Ca phases. Figure 3a shows the XANES spectra for several Ca reference compounds.
176 The four $CaCO_3$ species (calcite, vaterite, aragonite and amorphous $CaCO_3$ (ACC)) have clearly
177 distinct spectra, which enables their identification (14, 15). However, Ca XANES has no
178 sensitivity to substitutional impurities as seen for instance for low Cd-containing vaterite (Cd
179 content lower than 1%, as estimated by µXRF) and pure vaterite exhibiting nearly identical
180 spectra. The spectra for aqueous Ca^{2+}, Ca oxalate monohydrate and ACC share some similarities.
181 However, the lower part of the edge is shifted to lower energy for ACC spectrum, and the
182 maximum of the white line (zero value of the first derivative) increases from 4049.5 eV (ACC) to

183 4049.9 eV (Ca oxalate monohydrate) and to 4050.5 eV (aqueous Ca^{2+}, Fig. 3b). The aragonite
184 spectrum is distinct from the three previous spectra in displaying a shoulder at 4046 eV (arrow in
185 Fig. 3), and a minimum between 4060 and 4070 eV.
186 Figure 4 shows the Ca µXANES spectra for the grains. They were fitted by LC using the standard
187 spectra presented above, and results are presented in Table 2. The ZnCa3 spectrum presents
188 strong similarities with the aragonite spectrum, but markedly lower amplitude. The drop in
189 amplitude suggests some over-absorption effect (12) due to a high Ca content of the analyzed
190 spot. The fit without over-absorption correction (see materials and Methods) did not provide
191 satisfactory result (*NSS* = 0.065 %, with 68% vaterite + 25% aragonite). Introducing an over-
192 absorption correction greatly improved the fit (*NSS* = 0.014 % with aragonite as only component,
193 Fig. 4). The *a* value found (1.38) corresponds to a very strong over-absorption effect. The fit was
194 not improved significantly by introducing a second component (*NSS* decreased by less than
195 10%). Thus, the spot analyzed by µXANES likely contains aragonite as the sole Ca species.
196 The grains ZnCa4 and ZnCa5 were fitted with 98% calcite. The fit was slightly improved with a
197 correction of over-absorption (*NSS* = 0.015 and 0.021 %, compared to 0.020 and 0.035 %,
198 respectively), and the proportions were unchanged. Adding a second component did not improve
199 significantly the fits (*NSS* decreased by less than 10%).
200 For grain Zn2 and CdCa6, fits without over-absorption correction were not satisfactory (*NSS* =
201 0.048 and 0.091 %, respectively, for two-component fits). Fair one-component fits with over-
202 absorption correction were obtained with ACC (*NSS* = 0.021 and 0.024 %, respectively), but the
203 match was not optimal for the first oscillation (around 4080 eV). Ca oxalate monohydrate and
204 aqueous Ca^{2+} provided weaker fits (*NSS* = 0.086 and 0.053 % for Zn2, and 0.076 and 0.043 % for
205 CdCa6, respectively). Adding a second component did improve the reproduction of the first
206 oscillation. Several fits of equivalent qualities were obtained with ACC as major component

(about 80 and 70 % of total Ca) and various species as secondary component. *NSS* values were more than doubled if ACC was excluded (Table 2 and Fig. 1 in Supplemental Information). Therefore, grains Zn2 and CdCa6 likely contain ACC as major species, and an additional species whose nature remains unknown.

For the other grains (Zn3, CdCa2, CdCa3 and Cd10), over-absorption correction did not improve the fits. Calcite was the major form in grains Zn3 and CdCa2, and fits of equivalent quality were obtained with ACC, aqueous Ca^{2+} and Ca oxalate monohydrate as minor species. Aqueous Ca^{2+} is unlikely in solid-state material. ACC and Ca oxalate monohydrate are more likely. In the absence of reference spectra for Ca bound to organic ligands other than oxalate, this latter compound may be considered as a proxy for Ca bound to organic compounds in general. Therefore, this pool is referred to as "organic Ca and/or ACC" in Table 3. Vaterite was found in grains CdCa3 and Cd10. For this latter grain only, no satisfactory fit was obtained with two components (*NSS* = 0.046 %), so a third component was introduced. Again, a contribution of organic Ca and/or ACC was found in grains CdCa3 and Cd10.

The speciation of Ca was then compared with the mineralogy and morphology of the grains (Table 3). The percentages were rounded to the nearest ten for clarity. Except for two grains, ZnCa3 and CdCa2, the same crystalline species were identified by µXRD and Ca µXANES. Zn-substituted calcite and Cd-substituted vaterite were identified by µXRD in grains ZnCa3 and CdCa2, respectively, but not by Ca µXANES spectroscopy. This difference likely results from the larger beam size and higher penetration depth of X-rays in XRD measurements relative to µXANES (16 × 7 µm *vs* 5 × 5 µm, and a few tens of µm at 17 keV *vs*. a few µm at 4 keV). Thus,

229 XRD probes a different material volume than Ca μXANES even when conducted on the same
230 spot.
231
232 **Discussion and Conclusion**
233 Results showed that beside crystalline calcium carbonates (calcite, vaterite and aragonite), the
234 tobacco grains contained ACC as well. Whewellite (Ca oxalate monohydrate) did show up in
235 some XANES fits, but its presence could not be firmly attested. Ca oxalate mono- and dihydrate
236 have several XRD peaks in common with calcite, but peaks at distinct positions as well. These
237 two minerals were positively identified by μXRD in other tobacco grains based on the presence
238 of these specific peaks (3). In the present study, no such peaks were found on the XRD patterns.
239 However, it is still possible that coarse crystals of Ca oxalate mono or dihydrate are present but
240 produce non-specific peaks only, or that Bragg conditions were not met for these coarse crystals.
241 Therefore, the presence of Ca oxalate mono- and dihydrate cannot be ruled out. Other
242 undetermined organic ligands may also complex Ca. In addition, mixed mineral and organic Ca
243 compounds such as organic matter-containing calcite (16) may occur.
244 The Ca μXANES analysis showed that strong over-absorption effects may take place and
245 decrease dramatically the amplitude of the spectra. We show that this effect is far from negligible
246 when identifying and quantifying Ca species. For instance, for grain ZnCa3, the uncorrected
247 spectrum was fitted by 68% vaterite + 25% aragonite, and the corrected spectrum was fitted with
248 100% aragonite. Note that the LCF without over-absorption correction was relatively bad, which
249 alerted us on the possibility of an over-absorption effect.
250 In the environment, ACC is thermodynamically unstable and rapidly transforms into vaterite and
251 then calcite (17). However, it is found as a stable compound in plants (e.g., cystoliths) and
252 animals (e.g., cuticle of crustaceans, spicules of ascidiae, granules in molluscs) (18). ACC is

253 probably stabilized by proteins, magnesium and phosphorus in these organisms (18). In our case,
254 Mg and P were found in the grains.
255 Biologically controlled biomineralization leads to well defined mineral species and shapes.
256 Here, the variety of morphologies and of $CaCO_3$ crystal structures, and their coexistence with
257 amorphous and possibly organic forms, supports the hypothesis of a biologically induced (as
258 opposed to biologically controlled) biomineralization. This study illustrates the potential of
259 microfocused X-ray techniques to study biomineralization processes, and strategies of metals
260 immobilization developed by plants to cope with metal toxicity.
261

262 **Acknowledgements**

263 We acknowledge the ALS (Berkeley, USA) and the ESRF (Grenoble, France) for the provision
264 of beamtime. We are grateful to Jean Susini and the staff of beamline ID21 at the ESRF for their
265 technical support during the experiment. The operations of the Advanced Light Source at
266 Lawrence Berkeley National Laboratory are supported by the Director, Office of Science, Office
267 of Basic Energy Sciences, Materials Sciences Division, of the US Department of Energy under
268 Contract No. DE-AC02-05CH11231. We acknowledge Y. Politi and S. Weiner for sharing the
269 ACC Ca XANES spectrum, and two anonymous reviewers.

References

1. Choi, Y. E., Harada, E., Wada, M., Tsuboi, H., Morita, Y., Kusano, T. & Sano, H. Planta **213**, 45-50 (2001).
2. Choi, Y. E., Harada, E., Kim, G. H., Yoon, E. S. & Sano, H. J. Plant Biol. **47**, 75-82 (2004).
3. Sarret, G., Harada, E., Choi, Y. E., Isaure, M. P., Geoffroy, N., Birschwilks, M., Clemens, S., Fakra, S., Marcus, M. A. & Manceau, A. Plant Physiol. **141**, 1021-1034 (2006).
4. Lowenstam, H. & Weiner, S. On Biomineralization (Oxford University Press, New York, Oxford, 1989).
5. Choi, Y. E. & Harada, E. J. Plant Biol. **48**, 113-119 (2005).
6. Paquette, J. & Reeder, R. J. Geochim. Cosmochim. Acta **59**, 735–749 (1995).
7. Reeder, R. J. Geochim. Cosmochim. Acta **60**, 1543–1552 (1996).
8. Politi, Y., Levi Kalisman, Y., Raz, S., Wilt, F., Addadi, L., Weiner, S. & Sagi, I. Adv. Funct. Mat. **16**, 1289-1298 (2006).
9. Marcus, M. A., MacDowell, A. A., Celestre, R., Manceau, A., Miller, T., Padmore, H. A. & Sublett, R. E. J. Synchrotron Rad. **11**, 239-247 (2004).
10. West, A. Solid State Chemistry and its Applications (Wiley, New York, 1984).
11. Ressler, T. J. Phys. IV **7**, c2-269 (1997).
12. Manceau, A., Marcus, M. A. & Tamura, N. in Applications of Synchrotron Radiation in Low-Temperature Geochemistry and Environmental Science (eds. Fenter, P., Rivers, M., Sturchio, N. & Sutton, S.) 341-428 (Reviews in Mineralogy and Geochemistry, Mineralogical Society of America, Washington, DC., 2002).
13. Shannon, R. D. Acta Crystallogr. A **32**, 751-767 (1976).
14. Levi Kalisman, Y., Raz, S., Weiner, S., Addadi, L. & Sagi, I. Adv. Funct. Mat. **12**, 43-48 (2002).
15. Pattanaik, S. Nucl. Inst. Meth. Phys. Res. B **229**, 367-374 (2005).
16. Phillips, B. L., Lee, Y. J. & Reeder, R. J. Environ. Sci. & Technol. **39**, 4533-4539 (2005).
17. Ogino, T., Suzuki, T. & Sawada, K. J. Cryst. Growth **100**, 159-67 (1990).
18. Weiner, S., Levi Kalisman, Y., Raz, S. & Addadi, L. Connective Tissue Research **44 Suppl. 1**, 214-218 (2003).

Table 1. Tobacco culture conditions and name of the grains investigated

Treatment conditions	Cation Concentrations in the Nutrient Solution (mM)			Grain Names	Techniques and References				
	Ca	Zn	Cd		SEM-EDX	µXRD	Zn µEXAFS	Cd µXANES	Ca µXANES
Zn	0.28	0.25	0	Zn2	(3) and this paper	(3)	(3)	-	this paper
				Zn3	-	this paper	unpubl.	-	
Zn + Ca	3.28	0.25	0	ZnCa3	(3) and this paper	(3)	(3)	-	this paper
				ZnCa4	(3) and this paper	(3)	(3)	-	this paper
				ZnCa5	-	this paper	unpubl.	-	this paper
Cd	0.28	$0.08\ 10^{-3}$	0.025	Cd10	(a)	(a)	-	(a)	this paper
Cd + Ca	3.28	$0.08\ 10^{-3}$	0.025	CdCa2	(a)	(a)	-	(a)	this paper
				CdCa3	(a)	(a)	-	(a)	this paper
				CdCa6	(a)	(a)	-	(a)	this paper
Ca	3.28	$0.08\ 10^{-3}$	0	Ca3	this paper	-	-	-	-

(a) Isaure et al., in prep.

Table 2. Ca µXANES Results

Treatment	Grain Name	*a* [1]	Proportion of Ca species (%) Determined by Linear Combination Fitting the µXANES Spectra							
			Calcite	Vaterite	Aragonite	Amorphous $CaCO_3$	Aqueous Ca^{2+}	Ca oxalate 1 H_2O	Sum	*NSS* (%) [2]
Zn+Ca	ZnCa3	1.38			97 ± 2				97	0.014 [3]
	ZnCa4	0.12	98 ± 2						98	0.015 [3]
	ZnCa5	0.17	98 ± 2						98	0.021 [3]
Zn	Zn2	0.27			22 ± 10	76 ± 15			97	0.011 [3]
		0.27				77 ± 15		20 ± 15	97	0.016
		0.27				79 ± 15	17 ± 15		96	0.019
		0.42				(excluded)	55 ± 15	45 ± 15	100	0.050
	Zn3		62 ± 5			29 ± 5			91	0.009 [3]
			70 ± 5					22 ± 5	92	0.016
			71 ± 5				21 ± 5		92	0.018

Cd+Ca	CdCa2		85 ± 5		13 ± 5			98	0.012 [3]
			87 ± 5				10 ± 5	97	0.014
			89 ± 5			9 ± 5		98	0.015
	CdCa3			77 ± 5	21 ± 7			98	0.031 [3]
				79 ± 5			20 ± 7	99	0.036
				82 ± 5		16 ± 7		98	0.037
	CdCa6	0.38			74 ± 15		25 ± 15	99	0.015 [3]
		0.42			68 ± 15	32 ± 15		100	0.019
		0.28			(excluded)	73 ± 15	25 ± 15	98	0.040
Cd	Cd10		29 ± 7	42 ± 8		25 ± 5		96	0.022 [3]
			25 ± 7	37 ± 8	34 ± 5			96	0.025
			28 ± 7	42 ± 8			26 ± 5	96	0.028

[1] Coefficient of over-absorption. [2] Residual between fit and experimental data $NSS = \Sigma(\mu_{experimental} - \mu_{fit})^2 / \Sigma(\mu_{experimental})^2 \times 100$ in the 4000-4150 eV range, where μ is the normalized absorbance. [3] Fit shown in Fig. 4. The error bars on the percentages correspond to the variation needed to increase *NSS* by 20%.

Table 3. Summary of the information obtained on each grain[1]

Treatment	Grain Name	Ca Speciation (µXANES Results) [1]	Mineralogy (µXRD Results)	Aspect of the Grain (SEM Results)
Zn+Ca	ZnCa3	100% aragonite	Aragonite, Zn-subst. calcite ($Ca_{0.93}Zn_{0.07}CO_3$)	faceted
	ZnCa4	100% calcite	Zn-subst. calcite ($Ca_{0.87}Zn_{0.13}CO_3$)	faceted
	ZnCa5	100% calcite	Zn-subst. calcite ($Ca_{0.95}Zn_{0.05}CO_3$)	not observed
Zn	Zn2	80% ACC + 20% undetermined	No diffraction peaks	rounded
	Zn3	70% calcite + 30% organic Ca and/or ACC	Zn-subst. calcite ($Ca_{0.89}Zn_{0.11}CO_3$)	not observed
Cd+Ca	CdCa2	90% calcite + 10% organic Ca and/or ACC	Cd-subst. calcite, Cd-subst. vaterite	not observed
	CdCa3	80% vaterite + 20% organic Ca and/or ACC	Cd-subst. vaterite	rounded
	CdCa6	70% ACC + 30% undetermined	No diffraction peaks	not observed
Cd	Cd10	30% calcite + 40% vaterite + 30% organic Ca and/or ACC	Cd-subst. calcite, Cd-subst. vaterite	rounded + faceted

[1] The error bar on the percentages varies from 5 to 15% depending on the species (see Table 2)

Figure Captions

Figure 1: SEM imaging for the grains ZnCa3 (a), ZnCa4 (b) Zn2 (c), CdCa3 (d) and grain Ca3 (e), and EDX analyses were performed on the spots marked by a black cross.

Figure 2: μXRF spectrum (a) one- and two-dimensional μXRD patterns (b) for grain ZnCa5 and Zn3. All XRD peaks were attributed to substituted calcite. The positions of three peaks for pure calcite are indicated by arrows.

Figure 3: Ca K-edge XANES spectra for the reference compounds used in the linear combination fits (a) and zoom on the main peak for aqueous Ca2+, Ca oxalate monohydrate and ACC (b).

Figure 4: Ca K-edge μXANES spectra for the tobacco grains and corresponding linear combination fits. Five spectra (Zn2, CdCa6, ZnCa3, ZnCa5 and ZnCa4) were corrected for over-absorption.

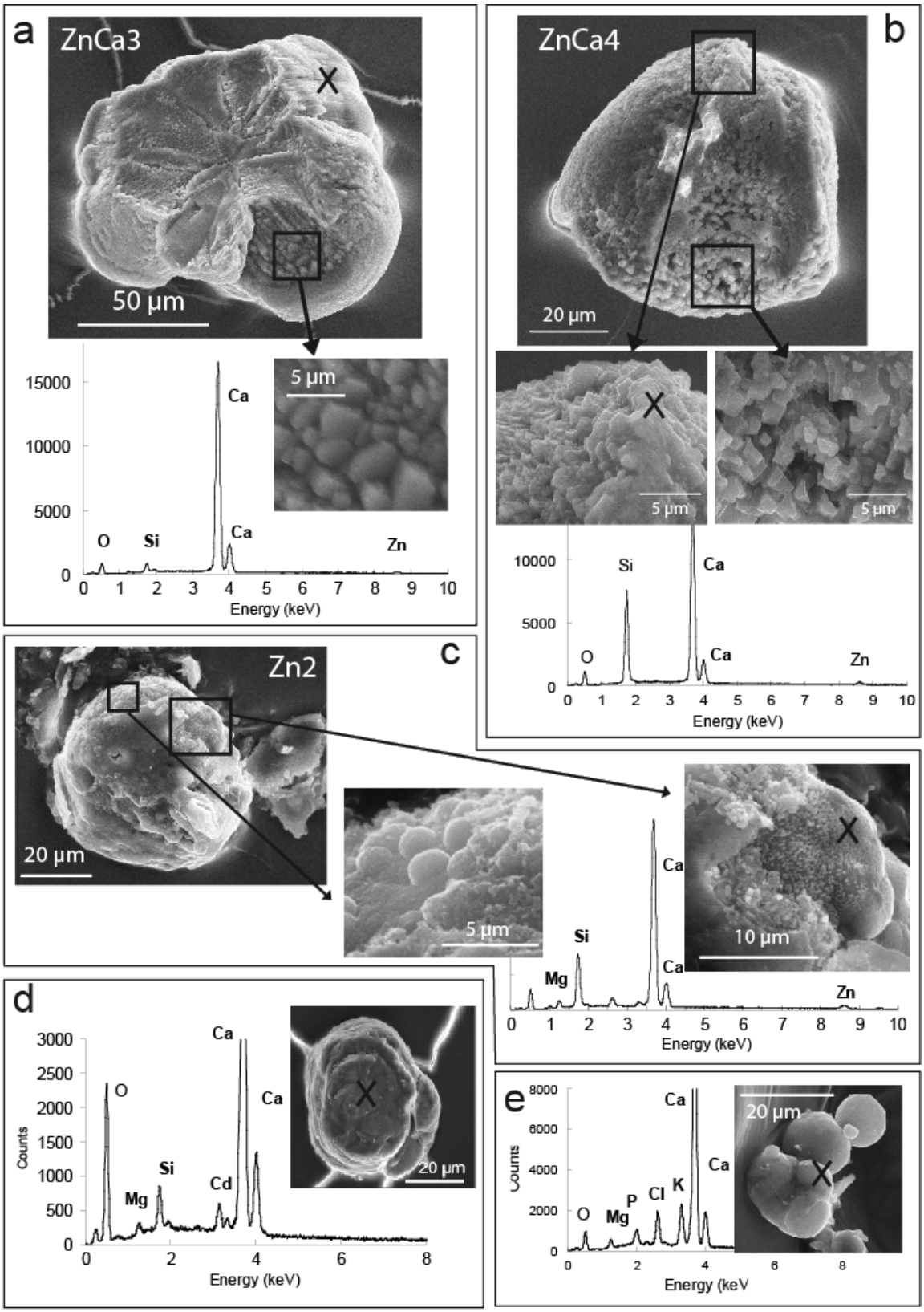
a
ZnCa3
50 µm
5 µm
Ca
O
Si
Ca
Zn
Energy (keV)
b
ZnCa4
20 µm
5 µm
5 µm
Si
Ca
O
Ca
Zn
Energy (keV)
c
Zn2
20 µm
5 µm
10 µm
Ca
Si
Mg
Ca
Zn
Energy (keV)
d
Counts
O
Ca
Ca
Si
Mg
Cd
20 µm
Energy (keV)
e
Counts
Ca
Ca
O
Mg
P
Cl
K
20 µm
Energy (keV

Figure 1

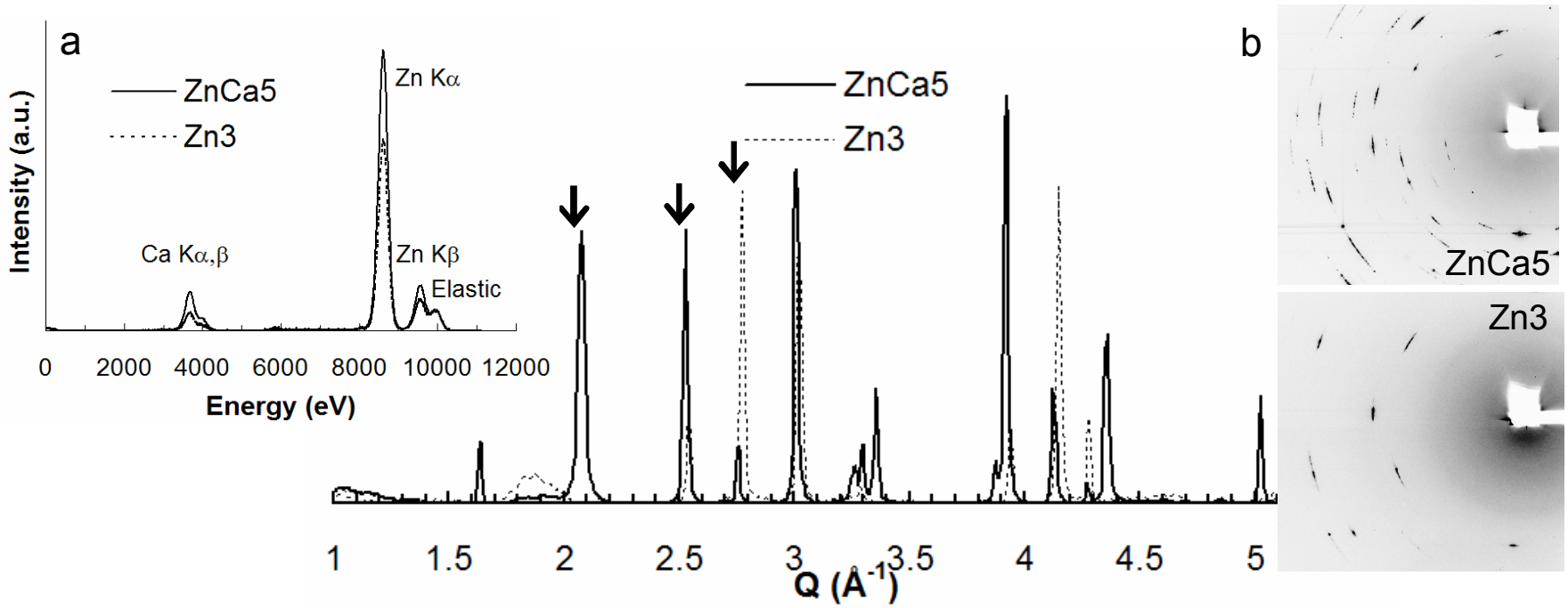
a
ZnCa5
Zn3
Intensity (a.u.)
Zn Kα
Ca Kα,β
Zn Kβ
Elastic
0
2000
4000
6000
8000
10000
12000
Energy (eV)
ZnCa5
Zn3
1
1.5
2
2.5
3
3.5
4
4.5
5
Q (Å-1)
b
ZnCa5
Zn3

Figure 2

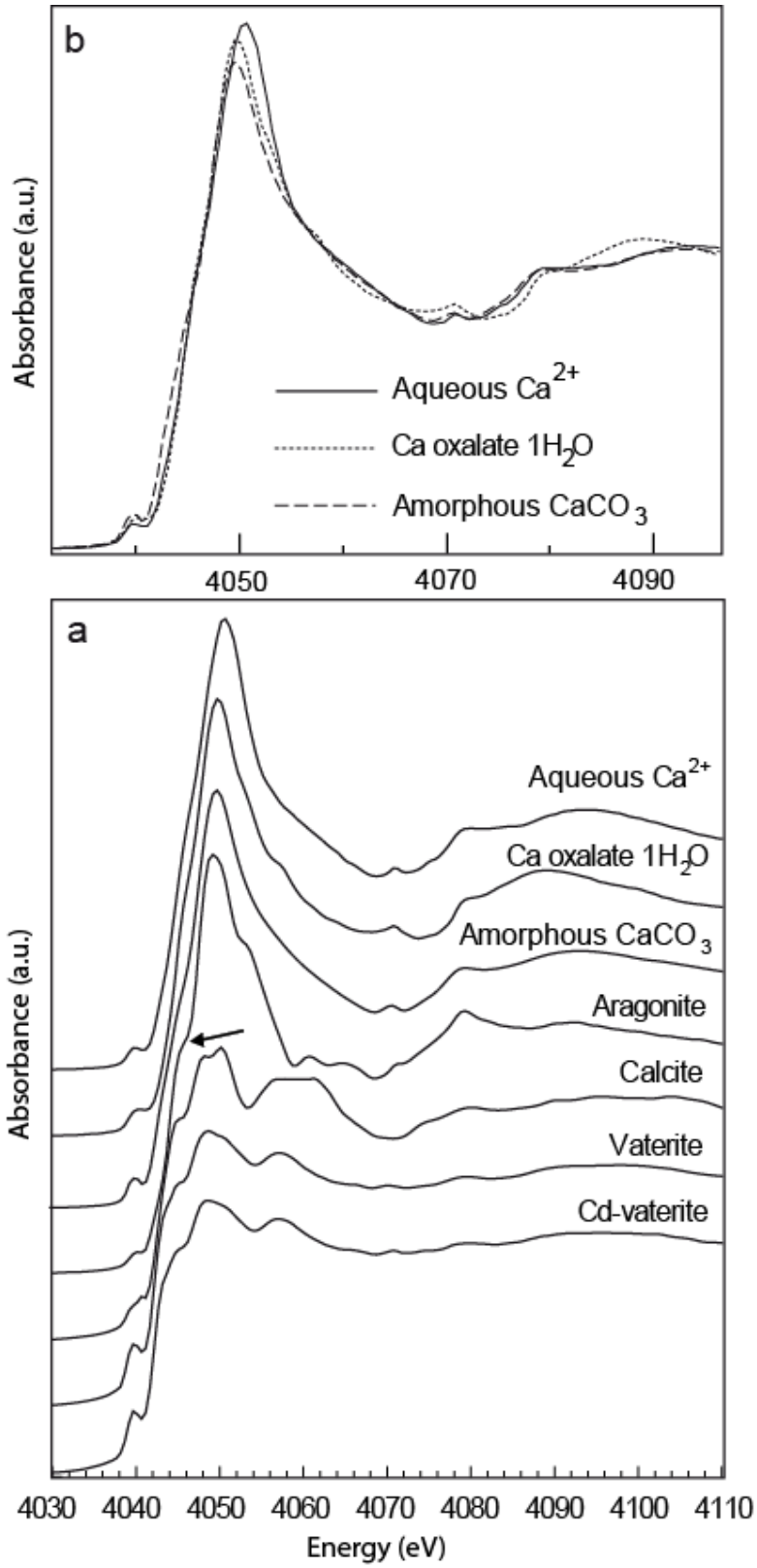
b
Absorbance (a.u.)
Aqueous Ca2+
Ca oxalate 1H2O
Amorphous CaCO3
4050
4070
4090
a
Absorbance (a.u.)
Aqueous Ca2+
Ca oxalate 1H2O
Amorphous CaCO3
Aragonite
Calcite
Vaterite
Cd-vaterite
4030 4040 4050 4060 4070 4080 4090 4100 4110
Energy (eV)

Figure 3

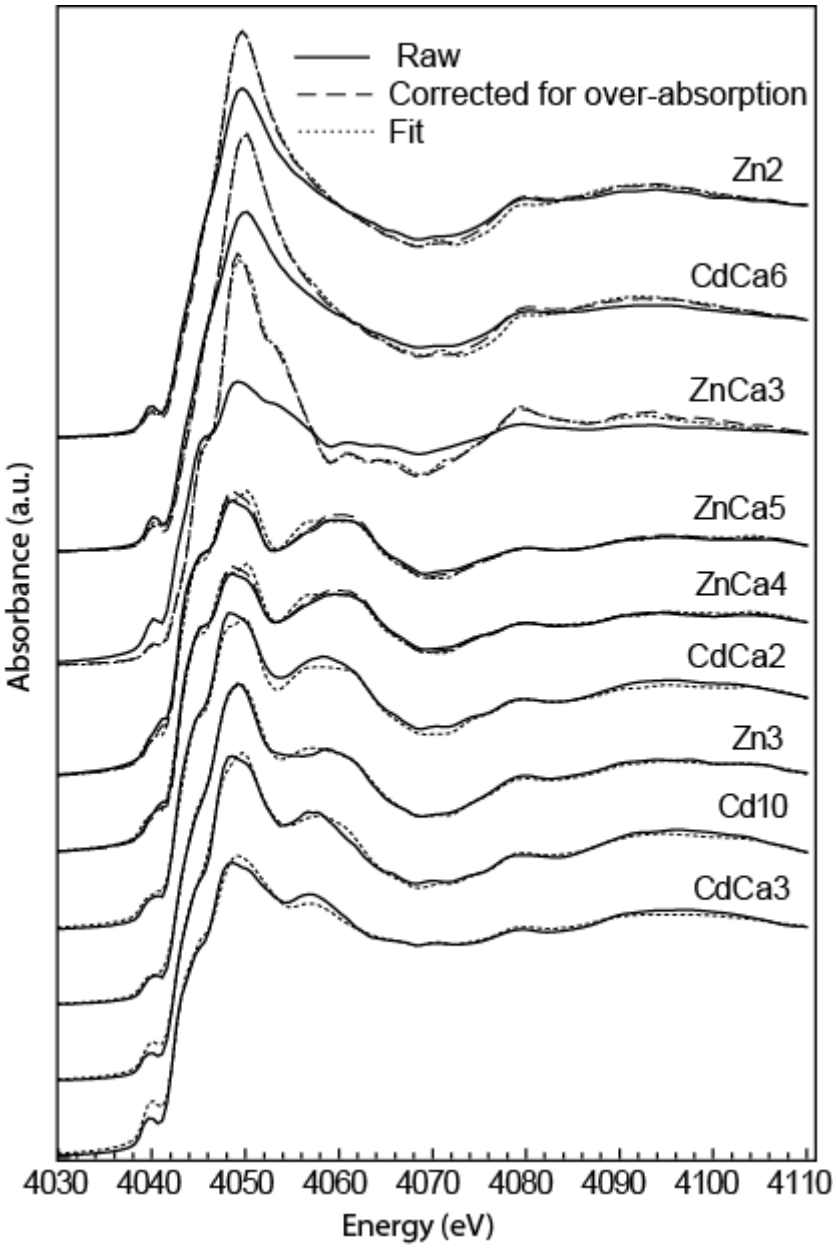
Raw
Corrected for over-absorption
Fit
Zn2
CdCa6
ZnCa3
ZnCa5
ZnCa4
CdCa2
Zn3
Cd10
CdCa3
Absorbance (a.u.)
4030
4040
4050
4060
4070
4080
4090
4100
4110
Energy (eV)

Figure 4

Supplemental information

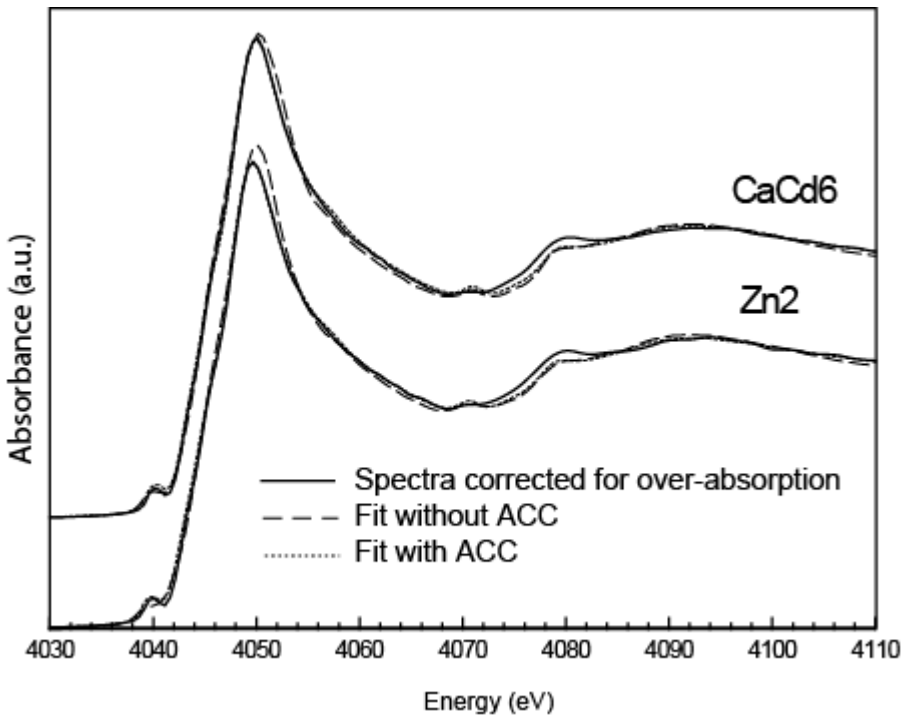

Figure 1: Comparison of the best two-component fits obtained for CaCd6 and Zn2 with and without ACC.